catalysts

MDPI

Article

Catalytic Ozonation of Norfloxacin Using Co-Mn/CeO_2 as a Multi-Component Composite Catalyst

Ruicheng Li [1,2], Jianhua Xiong [1,2,*], Yuanyuan Zhang [1,2,3,*], Shuangfei Wang [2], Hongxiang Zhu [2] and Lihai Lu [4]

1 School of Resources, Environment and Materials, Guangxi University, Nanning 530004, China
2 Guangxi Key Laboratory of Clean Pulp and Papermaking and Pollution Control, College of Light Industry and Food Engineering, Guangxi University, Nanning 530004, China
3 School of Marine Sciences, Guangxi University, Nanning 530004, China
4 Guangxi Bossco Environmental Protection Technology Co., Ltd., Nanning 530007, China
* Correspondence: happybear99@126.com (J.X.); jiedeng05@sina.com (Y.Z.)

Abstract: In this study, a Co-Mn/CeO_2 composite was prepared through a facile sol-gel method and used as an efficient catalyst for the ozonation of norfloxacin (NOR). The Co-Mn/CeO_2 composite was characterized via XRD, SEM, BET and XPS analysis. The catalytic ozonation of NOR by Co-Mn/CeO_2 under different conditions was systematically investigated, including the effect of the initial solution's pH, Co-Mn/CeO_2 composite dose, O_3 dose and NOR concentration on degradation kinetics. Only about 3.33% of total organic carbon (TOC) and 72.17% of NOR could be removed within 150 min by single ozonation under the conditions of 60 mg/L of NOR and 200 mL/min of O_3 at pH= 7 and room temperature, whereas in the presence of 0.60 g/L of the Co-Mn/CeO_2 composite under the same conditions, 87.24% NOR removal was obtained through the catalytic ozonation process. The results showed that catalytic ozonation with the Co-Mn/CeO_2 composite could effectively enhance the degradation and mineralization of NOR compared to a single ozonation system alone. The catalytic performance of CeO_2 was significantly improved by the modification with Mn and Co. Co-Mn/CeO_2 represents a promising way to prepare efficient catalysts for the catalytic ozonation of organic polluted water. The removal efficiency of NOR in five cycles indicates that Co-Mn/CeO_2 is stable and recyclable for catalytic ozonation in water treatment.

Keywords: antibiotics; catalytic ozonation; emerging contaminant; Co-Mn/CeO_2; norfloxacin

check for updates

Citation: Li, R.; Xiong, J.; Zhang, Y.; Wang, S.; Zhu, H.; Lu, L. Catalytic Ozonation of Norfloxacin Using Co-Mn/CeO_2 as a Multi-Component Composite Catalyst. *Catalysts* **2022**, *12*, 1606. https://doi.org/10.3390/catal12121606

Academic Editor: Luigi Rizzo

Received: 27 October 2022
Accepted: 5 December 2022
Published: 8 December 2022

1. Introduction

Recently, the wide applications of antibiotics have become a serious threat to the environment and public health worldwide due to their resistance to degradation and induction of resistance genes [1,2]. Norfloxacin (NOR), a typical fluoroquinolone (FQ) antibiotic, has been widely used and found in wastewater treatment plants from different routes. For instance, the concentrations of NOR detected from domestic and hospital effluents range from ng/L to μg/L [3,4]. It was found that NOR concentrations could even reach up to mg L^{-1} in pharmaceutical effluents [5]. Nevertheless, antibiotics might have a potential adverse influence on aquatic wildlife and humans even at trace levels [6]. Therefore, it is crucial to remove NOR efficiently from the aquatic environment.

Advanced oxidation processes (AOPs), which include several techniques, can generate highly oxidative species to mineralize antibiotics [7,8]. Among them, ozonation has been widely applied for the oxidative degradation of pollutants. Ozone (O_3) as a powerful oxidizing agent could degrade many organic pollutants including fluoroquinolone antibiotics. However, because of its selective oxidization of organic matters, the mineralization efficiencies of some antibiotics were relatively low when a single ozonation system was used [9,10]. A heterogeneous catalytic ozonation process could effectively improve the degradation of organic pollutants and has attracted significant attention in recent years. The heterogeneous catalysts for ozonation, such as metal oxides (MnO_2, Al_2O_3, Fe_3O_4, Co_3O_4

and CuO), metal-containing composites and carbon materials have been developed and applied in catalytic ozonation systems for the removal of various organic pollutants [11–16]. Among them, MnO_2 has been investigated and reported as a promising catalyst for O_3 due to its high efficiency and stability. For example, Nawaz et al. investigated the degradation of 4-nitrophenol (4-NP) through a heterogeneous catalytic ozonation process by using MnO_2 as the catalyst. Under the same reaction conditions, the degradation efficiency of MnO_2-catalyzed catalytic ozonation was 60.5% higher than that of ozonation alone [13]. The catalysis may be partly attributed to the role of oxygen vacancies (OVs) on MnO_2. As reported by He et al., oxygen vacancies facilitate the adsorption of O_3 onto the catalyst surface because oxygen vacancies increase the ratio of Mn^{3+}/Mn^{4+}, and then alter the charge distribution [17]. Meanwhile, Co_3O_4 also exhibited high catalytic activity for the catalytic ozonation of various refractory organic compounds. For example, Alvarez et al. investigated the degradation of pyruvic acid through a heterogeneous catalytic ozonation process by using Co_3O_4/Al_2O_3 composites as the catalyst. Under the same reaction conditions, the degradation efficiency of Co_3O_4-/Al_2O_3-catalyzed catalytic ozonation was 38% higher than that of ozonation alone. The rate of pyruvic acid disappearance is improved by the presence of cobalt, which is likely due to its catalytic effect on oxidation reactions [18].

Cerium oxides (CeO_2) has been widely applied in many research areas such as CO oxidation, VOC combustion and the water-gas shift reaction due to a low redox potential and abundant OVs [19–23]. In recent years, CeO_2, as an active component or support, has been widely investigated as an ozonation catalyst to enhance the removal of recalcitrant compounds [24–26]. For example, Li et al. found that ceria could accelerate MCM-48 to strengthen the degradation efficiency of clofibric acid (CA) by O_3 [27]. Akhtar et al. found that the presence of Fe_2O_3/CeO_2 could accelerate activated carbon to enhance the removal efficiency of sulfamethoxazole by O_3 [26]. Chen et al. reported that the introduction of a ceria catalyst can significantly enhance the catalytic ozonation of 4-chlorophenol, which could be attributed to the concentration and location of OVs [25]. However, few studies have reported on the combination of CeO_2 and Co-Mn for organic pollutant elimination via catalytic ozonation.

In this work, the Co-Mn/CeO_2 composite was fabricated by using the sol-gel method. The physical properties of the catalyst, the heterogeneous catalytic ozonation activities of Co-Mn/CeO_2 for the degradation of NOR, the performance of various operating conditions and the stability of the catalyst were evaluated.

2. Results and Discussion

2.1. Physical Properties of Catalysts

The crystal phases and crystallinities of CeO_2 and Co-Mn/CeO_2 catalysts were studied by using XRD. As shown in Figure 1a, the CeO_2 particles depicted the typical XRD patterns of pure fluorite cubic structures of CeO_2 (JCPDS 34-0349) with characteristic peaks at 2θ values of 28.6°, 33.1°, 47.5°, 56.4°, 59.1°, 69.5°, 76.8° and 79.1°, which were attributed to the (111), (200), (220), (311), (222), (400), (331) and (420) crystal planes, respectively [28–30]. The Co-Mn/CeO_2 composite samples did not show any obvious XRD diffraction for manganese oxides or cobalt oxides in Figure 1. Moreover, the XRD patterns of the Co-Mn/CeO_2 samples are quite broad compared to pristine CeO_2, which could be attributed to the formation of effective Mn-Ce, Co-Ce, and Mn- and Co-codoped solid solutions [23,31–33]. As the width and strength of XRD peaks have a close relationship with the crystallinity and crystal size of the corresponding crystal phase, the low crystallinity and small crystal size of metal oxide species can afford a large number of active sites for improved catalysis and provide a material basis for a high catalytic performance [32,34].

As shown in Figure 2a, it can be seen that the CeO_2 was in the form of irregular particles, which were evenly distributed, and there were many pores between the particles. The SEM image indicated that Co-Mn/CeO_2 was in the form of irregular flakes that were highly dispersed, and the surface was covered with a certain agglomeration and fluffy accumulation, as well as many pores with different sizes (Figure 2b). The above results

indicate that Co-Mn/CeO_2 has a hierarchal micro–meso–macro porous structure. These pores were formed due to the gasification of free water and the decomposition of nitrates which acted as pore-fabricating agents in the sol-gel combustion preparation process [35]. Furthermore, in order to confirm the composition of Co-Mn/CeO_2, EDS mapping was performed, and the elemental mappings are shown in Figure 2c. The results showed a uniform dispersion of Mn, Co, Ce and O elements in the Co-Mn/CeO_2 catalysts which were consistent with the XRD and SEM results. The loose, porous structure may provide more active sites for reactant molecules, thereby promoting the performance of the catalysts [34].

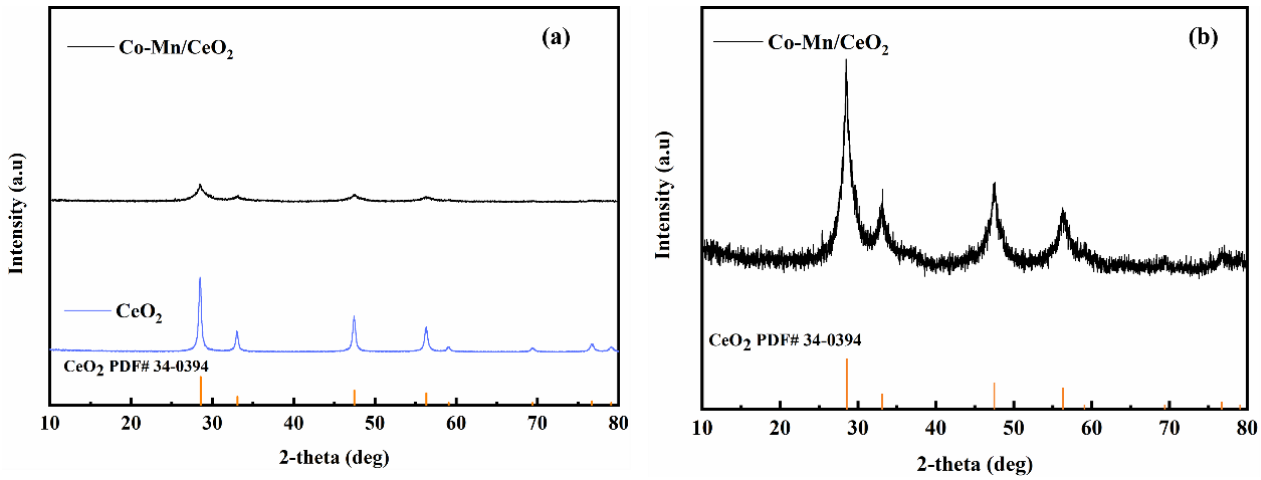

Figure 1. XRD pattern of CeO_2 and Co-Mn/CeO_2 (**a**); XRD patterns of pristine Co-Mn/CeO_2 (**b**).

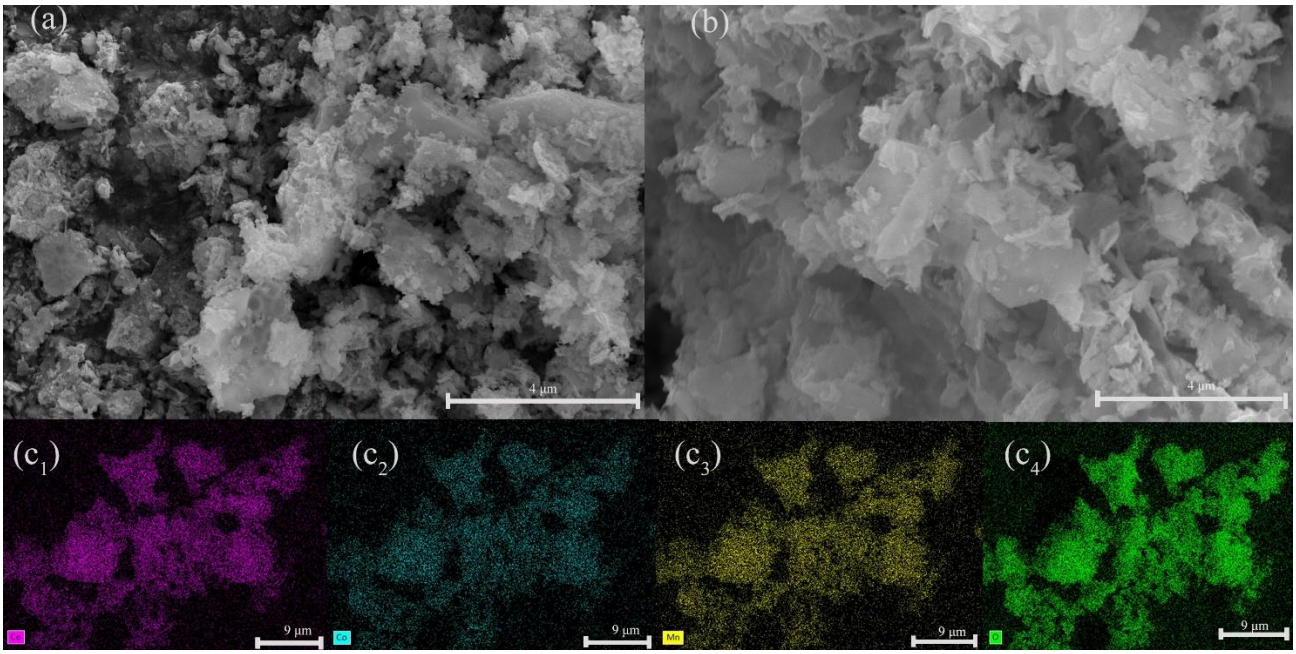

Figure 2. SEM images of CeO_2 (**a**), Co-Mn/CeO_2 (**b**), and EDS mapping of Co-Mn/CeO_2 (**c_1–c_4**).

As shown in Figure 3, the N_2 adsorption–desorption isotherms of CeO_2 and Co-Mn/CeO_2 were type IV, showing that the two materials contained microporous and mesoporous structures. The data on the surface area, pore diameter and pore volume are summarized in Table 1. The BET surface area significantly increased from 34.80 m^2/g (CeO_2) to 92.43 m^2/g (Co-Mn/CeO_2). Compared with CeO_2, Co-Mn/CeO_2 has the smaller average pore size and the larger pore volume, indicating that Co-Mn/CeO_2 has more pores.

The larger specific surface area and pore number of Co-Mn/CeO_2 may be attributed to the formation of OVs and surface defects, which can provide more active sites to enhance the catalytic performance [11,36,37].

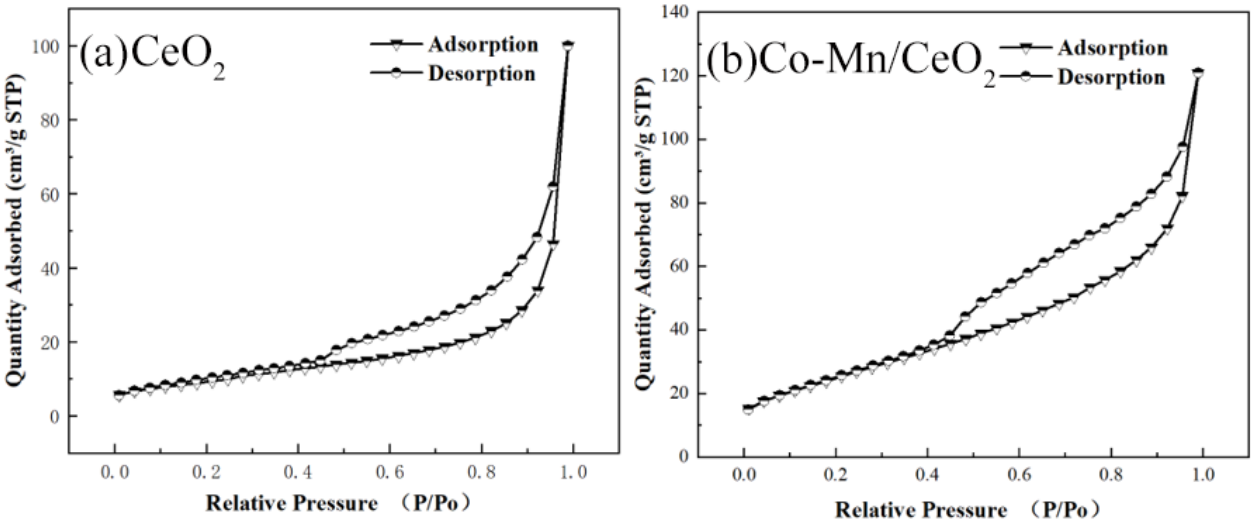

Figure 3. N_2 adsorption–desorption isotherms of CeO_2 (**a**); Co-Mn/CeO_2 (**b**).

Table 1. Surface area, average pore width and total pore volume of catalysts.

Catalyst	BET Surface Area (m^2/g)	Adsorption Average Pore Width (nm)	Total Pore Volume of Pore (cm^3/g)
CeO_2	34.804	17.8224	0.1551
Co-Mn/CeO_2	92.425	8.10891	0.1874

The element composition and chemical environment of CeO_2 and Co-Mn/CeO_2 were further identified by using XPS. As illustrated in Figure 4a, in addition to the characteristic peaks of Co2p and Mn2p, the Ce3d and O1s peaks were observed clearly in both XPS survey spectrums of CeO_2 and Co-Mn/CeO_2, which were consistent with the EDS results. For Co-Mn/CeO_2, there were two major peaks at $Co2p_{3/2}$ and $Co2p_{1/2}$, and the fitted peaks at 780.1 eV and 795.2 eV could be attributed to Co^{3+}, whereas the peaks at 781.5 eV and 796.4 eV could be ascribed to Co^{2+}. Thus, it is concluded that Co existed in the oxidation states of Co^{2+} and Co^{3+} [38]. As shown in Figure 4c, the Mn 2p XPS spectrum demonstrates two peaks centered at 642.4 eV and 653.5 eV, which can be attributed to Mn $2p_{3/2}$ and Mn $2p_{1/2}$ states, respectively [39]. The Mn $2p_{3/2}$ peak of Co-Mn/CeO_2 could be fitted by two main peaks centered at 642.3 eV and 644.1 eV with a ratio of 0.86, corresponding to the chemical states of Mn^{3+} and Mn^{4+}, respectively. The results show that the content of the Mn^{4+} species was higher than that of the Mn^{3+} species.

As shown in the Ce3d spectra of Figure 4b, the relative abundance of Ce 3d in Co-Mn/CeO_2 was smaller, suggesting that some Ce^{4+} in CeO_2 may be replaced by cobalt ions or manganese ions which could result in the creation of OVs. These principle binding energies were labeled as u and v, which were attributed to the two pairs of Ce spin-orbital doublets, $3d_{3/2}$ (higher BE) and $3d_{5/2}$ (lower BE), respectively. The photoelectron peaks u′ and v', u'' and v'', and u''' and v''' corresponded to the concentration of Ce^{4+}. Meanwhile, the two weak peaks labeled as u' and v' were ascribed as being characteristic of Ce^{3+} [1]. The relative concentration ratio of Ce^{3+} to Ce^{4+} can be calculated from the peak areas of deconvoluted peaks according to Equation (1)

$$r = \frac{A_{U'''} + A_{V'''} + A_{u''} + A_{v''} + A_U + A_V}{A_{U'} + A_{V'}} \quad (1)$$

The chemical valence state of Ce in CeO_2 and Co-Mn/CeO_2 mainly included the oxidation state of Ce^{4+} that coexisted with a relatively small amount of Ce^{3+}. The relative percentage of Ce^{3+}/Ce^{4+} of CeO_2 and Co-Mn/CeO_2 were then calculated to be 13.95% and 29.12%, respectively. As a defect indicator, the higher concentration of Ce^{3}+ in Co-Mn/CeO_2 indicated the creation of relatively more OVs on the surface of the catalyst [28,40,41].

The O1s results can further confirm the generation of abundant OVs. As shown in Figure 4e, the O1s spectrum of CeO_2 and Co-Mn/CeO_2 could be divided into three major components—529.5, 531.5 and 533.1 eV, which were assigned as lattice oxygen (denoted as O_{latt}), surface oxygen (O_{sur}) and adsorbed oxygen (O_{ads}), respectively. Generally, the surface oxygen species could improve the catalytic process [42,43]. The surface oxygen O_{sur} concentration of CeO_2 and Co-Mn/CeO_2 was 14.83% and 43.21%, respectively, indicating the same order as that of Ce^{3+}. These observations showed that combining Mn and Co with CeO2 not only promoted the formation of more new structure defects, but also improved the concentration of (O_{sur}) species, indicating that the Co-Mn/CeO_2 catalyst can provide more surface-active oxygen species for catalytic ozonation.

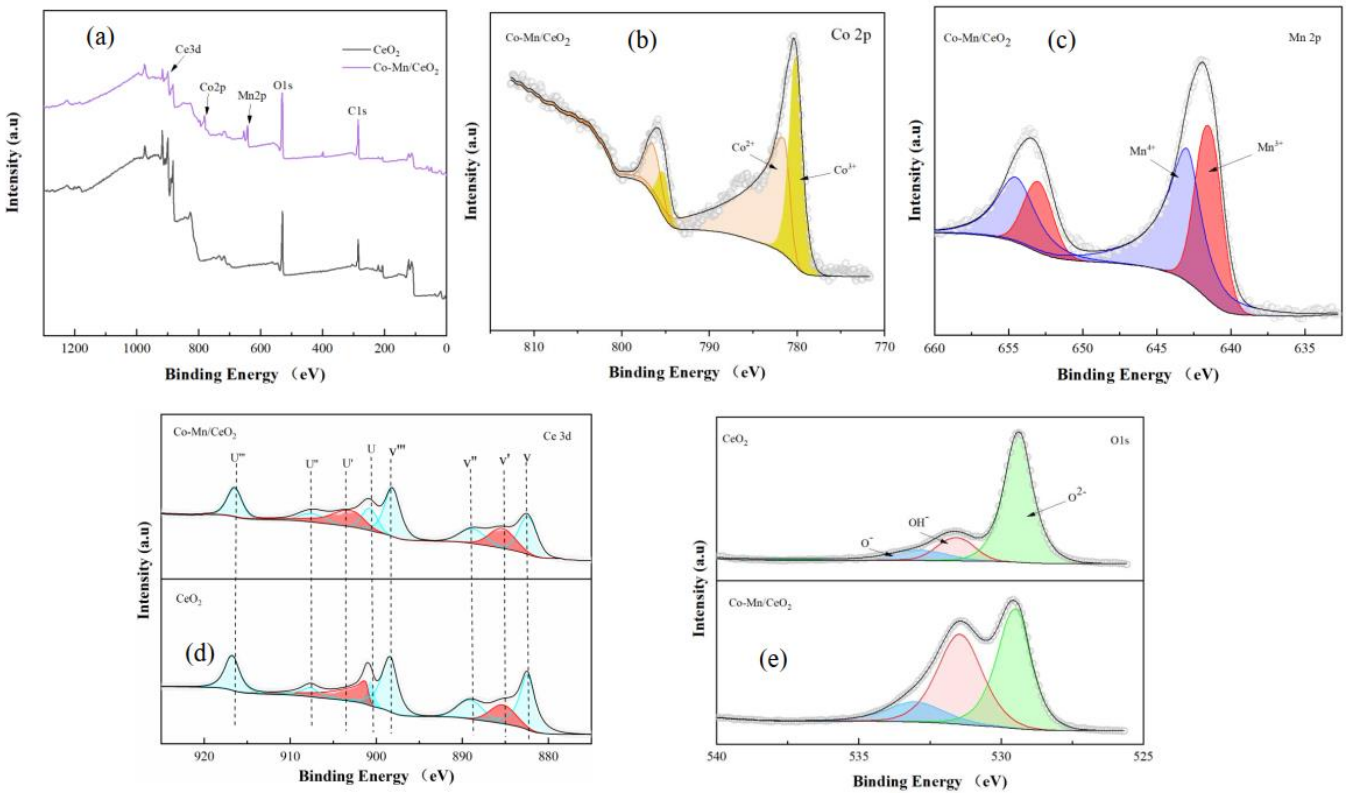

Figure 4. XPS survey spectra of CeO_2 and Co-Mn/CeO_2 (**a**); narrow region scan of Co2p (**b**), Mn2p (**c**), Ce3d (**d**) and O1s (**e**) of XPS spectra.

2.2. Catalytic Activities of Catalysts

To evaluate the performance of Co-Mn/CeO_2 in catalytic ozonation processes, NOR degradation and TOC removal in O_3, CeO_2/O_3 and Co-Mn/CeO_2/O_3 systems were investigated, and the results are shown in Figure 5. As shown in Figure 5a, the degradation efficiency of NOR via single ozonation was only 72.17% after 150 min. The efficiency increased to 76.15% and 87.24% in CeO_2 ozonation and Co-Mn/CeO_2 ozonation processes, respectively.

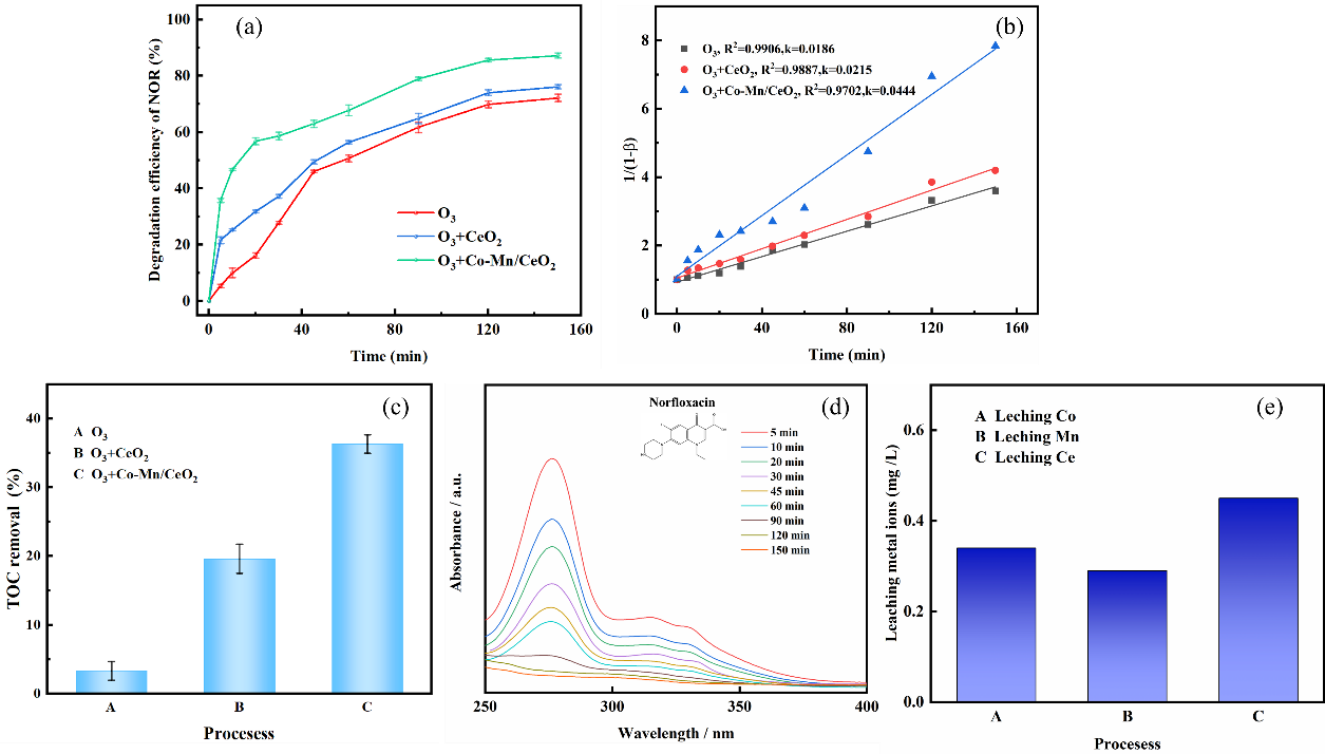

Figure 5. NOR degradation (**a**), quasi-second-order plot of NOR destruction, (**b**) TOC removal (**c**) in different processes, UV–vis spectra of treated water samples at different times (**d**); metal leaching amounts (**e**) (NOR = 60 mg/L; catalyst = 0.60 g/L; O_3 = 200 mL/min; initial pH of 7).

In order to further investigate the ozonation reaction kinetics, the experimental data were fitted with the second-order model (Equation (2)):

$$\frac{1}{1-\beta} = kc_0t + 1 \quad (2)$$

where k is the kinetic rate constant obtained from the fitting results. As shown in Figure 5b, the apparent first-order rate constant k of the NOR degradation was 0.0186 $(mg/L)^{-1}min^{-1}$, 0.0215 $(mg/L)^{-1}min^{-1}$ and 0.0444 $(mg/L)^{-1}min^{-1}$ in O_3, CeO_2/O_3 and Co-Mn/CeO_2/O_3 processes, respectively. It is worth noting that the different removal efficiencies of TOC were achieved with the addition of different catalysts. Moreover, these catalysts could significantly enhance the mineralization of NOR compared to the non-catalytic ozonation processes. Ozone, as a kind of oxidant, reacts easily with NOR, but due to its selective oxidation property, the ozone molecule might not be able to remove some degradation intermediates formed during NOR degradation, resulting in a low mineralization efficiency. As illustrated in Figure 5c, although NOR was effectively removed in 150 min by single ozonation, the removal efficiency of TOC was only about 3.33%. However, in the presence of CeO_2 and Co-Mn/CeO_2 under the same conditions, the removal efficiency of TOC increased to 19.61% and 36.31%, which was 1.9 and 10.9 times higher than that of the single ozonation and CeO_2/O_3 system, respectively. Figure 5d shows that the feature peak of NOR gradually disappeared within 180 min, indicating the complete degradation of NOR during the reaction. In addition, it can be noted in Figure 5e that catalysts had a low dissolution concentration of metal ions in the reaction solution after 150 min of reaction, which is acceptable according to discharge standards.

These results suggest that Co-Mn/CeO_2 had catalytic ozonation activity and can indeed strengthen the degradation of persistent organics. The main reason for this may be attributed to: (1) The doping of Co and Mn lead to the formation of surface defects and OVs,

which promote the decomposition of ozone into reactive radicals with stronger oxidation ability, and then achieve a better ozonation effect. (2) The electron transfer between Ce^{3+}/Ce^{4+}, Co^{3+}/Co^{2+} and Mn^{3+}/Mn^{4+} in Co-Mn/CeO_2 made the redox of Ce^{3+}/Ce^{4+} facile during the catalytic oxidation processes, improving the synergistic catalysis of Co, Mn and Ce for the degradation of NOR. This is consistent with the literature that shows Ce^{3+} species as the active sites in the decomposition of ozone into radicals with a more powerful oxidation ability [25].

2.3. Effect of Operational Conditions

2.3.1. Effect of Initial Solution pH

Figure 6 presents the effect of the initial solution's pH on NOR removal. The removal rate of NOR gradually increased with the increase in pH from the initial pH of 5.0 to 9.0, and the maximum NOR removal efficiency of 89.61% was achieved when the pH was 9.0. At a higher pH, the abundance of OH− could accelerate the decomposition of ozone into reactive radicals and enhance the generation of active radicals, such as hydroxyl radicals, leading to high NOR removal efficiency (Equations (3)–(7)):

$$O_3 + OH^- \rightarrow HO_4^- \quad (3)$$

$$HO_4^- \leftrightarrow HO_2\cdot + O_2^-\cdot \quad (4)$$

$$O_2\cdot + O_3 \rightarrow O_2 + O_3^-\cdot \quad (5)$$

$$O_3^-\cdot \rightarrow O_2 + O^-\cdot \quad (6)$$

$$O^-\cdot + H_2O \rightarrow \cdot OH + OH^- \quad (7)$$

However, as the initial pH further increased to 11.00, the NOR removal efficiency decreased because the enormous generation of •OH could facilitate the reaction between •OH itself or O^2•, rather than between the intermediate products of NOR degradation. The quasi-second-order kinetics fitting was performed on the removal of NOR molecules within 150 min. The results are shown in Figure 6b. The reaction rates were 0.0233 $(mg/L)^{-1}min^{-1}$, 0.299 $(mg/L)^{-1}min^{-1}$, 0.0439 $(mg/L)^{-1}min^{-1}$, 0.0554 $(mg/L)^{-1}min^{-1}$ and 0.0307 $(mg/L)^{-1}min^{-1}$. The results indicate that a low pH inhibited the reaction and slowed down the oxidation rate of NOR. When the pH value of the initial solution changed and was in the range of 3.00–11.00, NOR was almost removed in all cases. The results indicate that Co-Mn/CeO_2 can work in such a wide pH range.

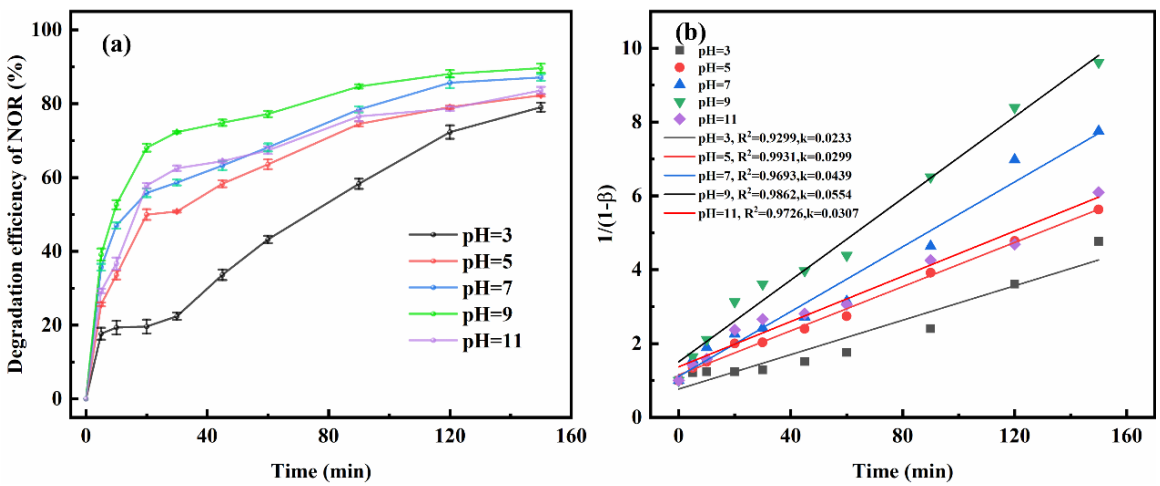

Figure 6. Effect of solution pH on NOR removal (**a**) and the kinetics equations and parameters of quasi-second-order reactions at different pH values (**b**) (if not otherwise specified, NOR = 60 mg/L; O_3 = 200 mL/min; Co-Mn/CeO_2 = 0.60 g/L).

2.3.2. Effect of O_3 Concentration

The increase in O_3 concentration could improve the removal of NOR, as shown in Figure 7. When the applied flow of O_3 was 100, 200 and 300 mL/min, the NOR removal efficiency within 150 min was 27.32%, 87.12% and 88.62%, respectively. The reaction rates were 0.0107 $(mg/L)^{-1}min^{-1}$, 0.0464 $(mg/L)^{-1}min^{-1}$ and 0.1347 $(mg/L)^{-1}min^{-1}$. The increase in NOR removal efficiency was due to the possibility of a higher concentration of O_3 accelerating the transformation of O_3 into the aqueous solution, forming more derived free radicals. However, when O_3 concentration increased from 200 mL/min to 300 mL/min, the reaction rate increased from 0.0464 $(mg/L)^{-1}min^{-1}$ to 0.1347 $(mg/L)^{-1}min^{-1}$. Since excess O_3 could also react with •OH to produce O_2 and H_2O, excess O_3 would compete with pollutants to react with free radicals, resulting in the decrease in oxidants for NOR removal (Equation (8)).

$$O_3 + 2{\cdot}OH \rightarrow 2O_2 + H_2O \quad (8)$$

Therefore, a high O_3 concentration may not always be conducive to the improving NOR removal.

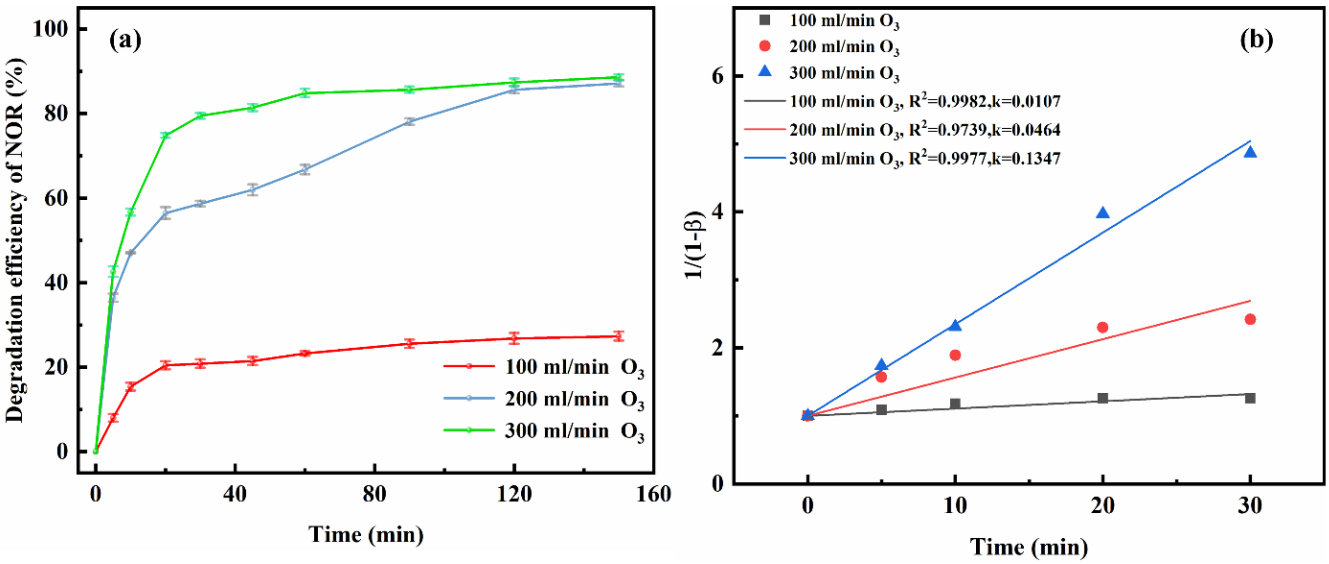

Figure 7. Effect of O_3 concentration on NOR removal (**a**) and the kinetics equations and parameters of quasi-second-order reactions at different O_3 concentrations (**b**) (if not otherwise specified, NOR = 60 mg/L; O_3 = 200 mL/min; Co-Mn/CeO_2 = 0.60 g/L; pH = 7).

2.3.3. Effect of Catalyst Dosage

Figure 8 shows the effect of Co-Mn/CeO_2 dosage on NOR removal. The removal of NOR gradually increased from 77.59% to 87.77% as the catalyst dosage increased from 0.4 to 0.8 g/L within 150 min. The reaction rate increased from 0.0222 $(mg/L)^{-1}min^{-1}$ to 0.0466 $(mg/L)^{-1}min^{-1}$. This might be due to the higher catalyst dose possibly providing more surface areas and available active sites, which could catalyze the disintegration of the ozone to produce more free active radicals in the oxidation process. However, the increase in NOR removal efficiency was only 6%, when Co-Mn/CeO_2 increased from 0.4 g/L to 0.6 g/L. In the presence of an excess catalyst, the concentration of NOR and O_3 per unit area might decrease, which was not conducive to the reaction between NOR and O_3 [28,44]. Hence, the optimized catalyst dosage was chosen as 0.6 g/L in this experiment.

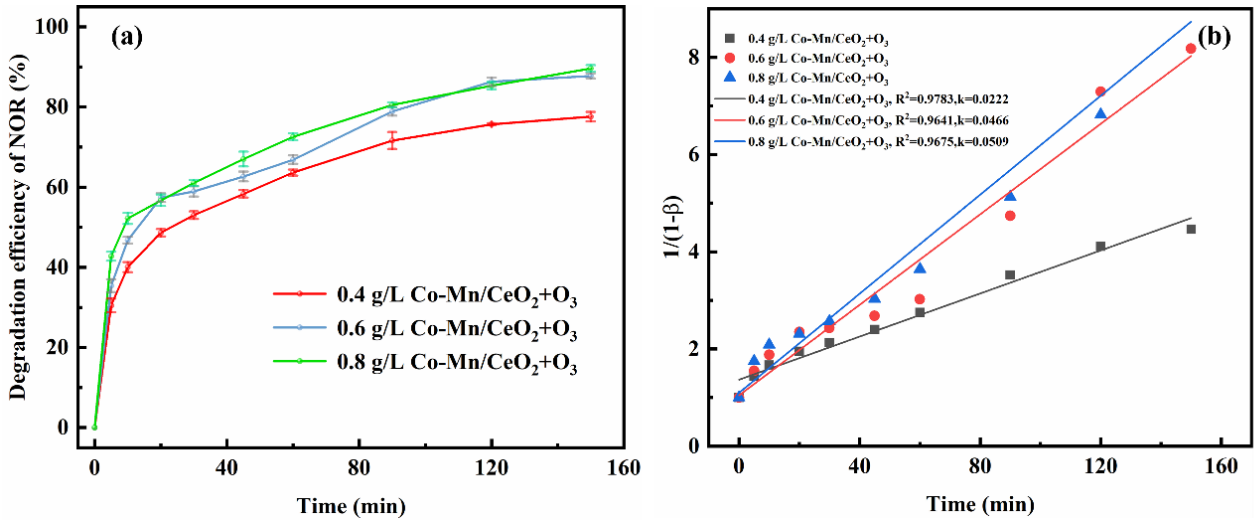

Figure 8. Effect of catalyst dosage on NOR removal (**a**) and the kinetics equations and parameters of quasi-second-order reactions at different catalyst dosages (**b**) (if not otherwise specified, NOR = 60 mg/L; O_3 = 200 mL/min; Co-Mn/CeO_2 = 0.60 g/L; pH = 7).

2.3.4. Effect of Initial NOR Concentration

Figure 9 presents the effect of the NOR initial concentration on NOR removal. When the initial concentration of NOR was 40 mg/L, 60 mg/L and 80 mg/L, the NOR removal efficiency was 86.51%, 87.65% and 79.39%, respectively. The reaction rates were 0.0562 $(mg/L)^{-1}min^{-1}$, 0.0456 $(mg/L)^{-1}min^{-1}$ and 0.0248 $(mg/L)^{-1}min^{-1}$. The results indicate that the degradation rate of norfloxacin was inhibited by the increase in NOR concentration. A higher concentration of pollutants may require more oxidants to be oxidized, and due to incomplete oxidation, intermediates will be produced and accumulate in the catalytic ozonation process, resulting in a low degradation efficiency [45].

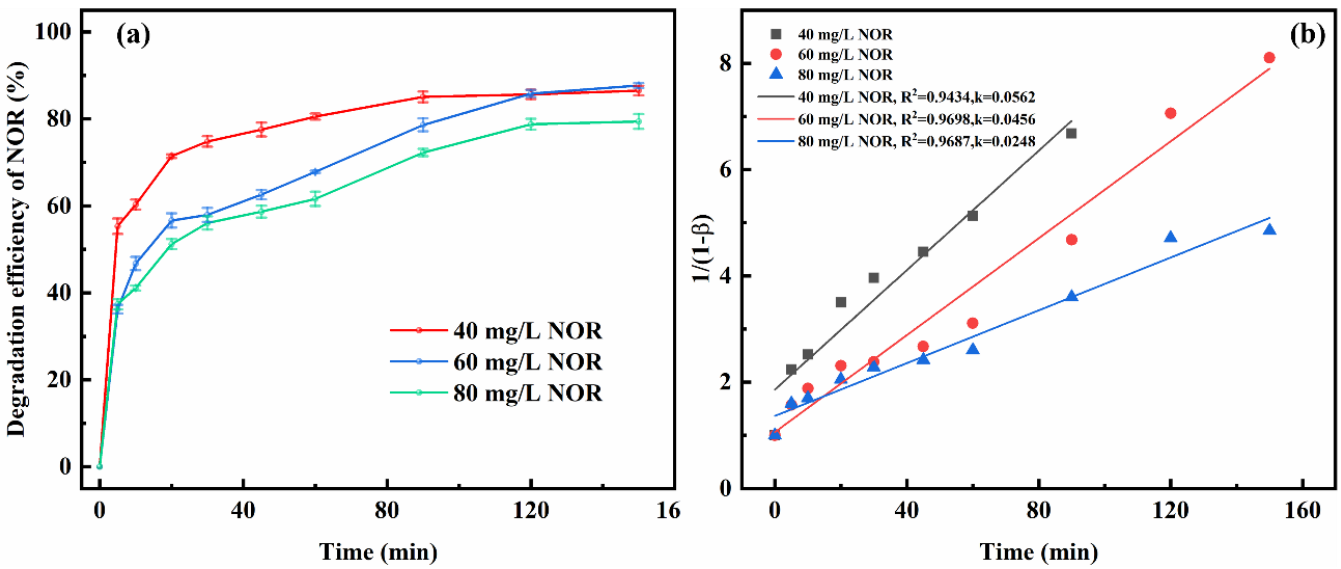

Figure 9. Effect of NOR initial concentration on NOR removal (**a**) and the kinetics equations and parameters of quasi-second-order reactions at different NOR initial concentrations (**b**) (if not otherwise specified, NOR = 60 mg/L; O_3= 200 mL/min; Co-Mn/CeO_2 = 0.60 g/L; pH = 7).

2.4. Catalyst Stability and Reusability

In order to evaluate the stability of Co-Mn/CeO_2 in the catalytic ozonation system, the catalyst was collected after each degradation reaction cycle and reused under the same operating conditions. As presented in Figure 10, the activity of Co-Mn/CeO_2 toward the degradation of NOR does not obviously change after five recycle times. This demonstrates that Co-Mn/CeO_2 had a stable performance in the catalytic ozonation process for the degradation of NOR.

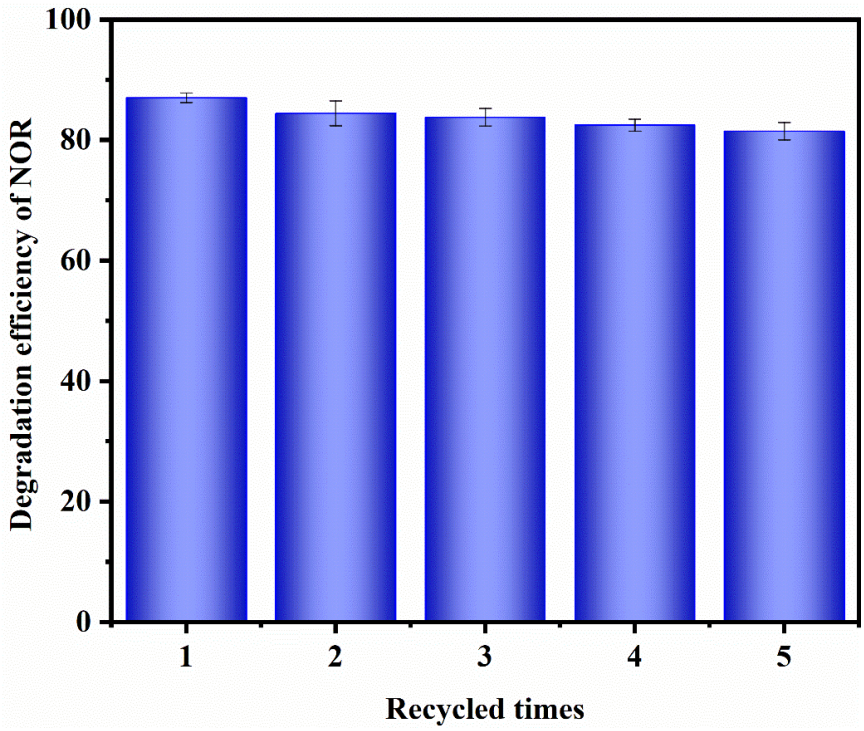

Figure 10. Stability of prepared Co-Mn/CeO_2 for the catalytic ozonation of NOR (if not otherwise specified, NOR = 60 mg/L; O_3 = 200 mL/min; Co-Mn/CeO_2 = 0.60 g/L; pH = 7; reaction time = 150 min).

3. Experimental Procedure

3.1. Materials and Chemicals

Norfloxacin (NOR) was purchased from Meilun Biotechnology Co., Ltd. (Dalian, China). Cobaltous nitrate ($Co(NO_3)_2 \cdot 6H_2O$), cerium nitrate ($Ce(NO_3)_3 \cdot 6H_2O$) and NaOH (Sodium hydroxide) were purchased from Aladdin Chemistry Co., Ltd (Shanghai, China). Manganese nitrate (50% *w/w*) and citric acid were bought from Guangzhou Chemical Reagent Co., Ltd. HCl (hydrochloric acid, 36%) was supplied by Lingfeng Chemical Reagent (Shanghai, China). Ultra-pure water, which was used as the experimental water, was obtained from the Millipore Milli-Q Ultrapure Gradient A10 purification system from Millipore Co., Ltd. (Burlington, MA, USA). All the chemicals and reagents used in the experiment were of analytical purity and could be used directly without further purification.

3.2. Preparation of Catalysts

The Co-Mn/CeO_2 catalyst was prepared by modifying the method described by [25]. Briefly, Co-Mn/CeO_2 was prepared by using the sol-gel method with citric acid as the chelating agent. Nitrate salts of cobalt, manganese and cerium, in addition to citric acid, were dissolved in deionized water with the molar ratio of Co(II): Mn(II): Ce(III): Citric acid = 1:1:1:3. Then, ammonia was added dropwise to adjust the pH to 4.5–5.0. The resulting solution was magnetically stirred at 80 °C until a viscous pale pink gel was formed. The gel was dried in an oven at 80 °C and then calcined in a muffle oven at 350 °C for 2 h.

The obtained black solid was stored in a dryer for further use. By comparison, CeO_2 was also prepared by adding the corresponding nitrate.

3.3. Ozonation Experiments

The ozonation experiment was carried out in a 150 mL glass column batch reactor. A certain amount of catalyst was added to the reactor containing 80 mL of NOR aqueous solution (the NOR test concentration was determined as 60 mg/L according to the relevant literature and experimental conditions [6,46,47], with an initial pH = 7), and then the mixed solution was maintained as a suspension by magnetic stirring. Next, the ozone gas was continuously bubbled to the bottom of the flask through the aeration device. Samples were collected from the ozone reactor within the prescribed time interval and then filtered using membrane filters (0.45 μm) for further analysis. Ozone gas was generated by using a Tonglin 3S-T3 ozone generator as the air source. Within the specified time interval, a certain volume of aliquots was taken from the reactor, and the residual ozone in the tail gas was removed with a sodium thiosulfate solution. Except for the test to investigate the influence of the initial pH value, other tests were conducted without adjusting the initial pH value. All the experiments were repeated at room temperature.

3.4. Characterization of Catalysts

X-ray diffraction (XRD) measurements were performed by using a D8 Discover Bruker diffractometer with Cu Kα radiation (Karlsruhe, Germany). The BET-specific surface areas were determined by using the AUTOSORB-IQ-MP system (Quantachrome, Boynton Beach, FL. USA). X-ray photoelectron spectroscopy (XPS, Waltham, MA, USA) spectra were determined via the Thermo Scientific K-Alpha system. The morphology was characterized by using an FEI Quattro S emission scanning electron microscopy (SEM, Waltham, MA, USA). Energy-dispersive spectroscopic (EDS) data were obtained by using the Bruker Quantax XFlash SDD 6 (Karlsruhe, Germany). An inductively coupled plasma optical emission spectrometry (ICP-OES, optima 8000DV, Waltham, MA, USA) was used to measure the leaching concentration of metal in the solution. The absorbance of NOR was measured with a UV-2700 spectrophotometer (Shimadzu, Kyoto, Japan) at 272 nm.

4. Conclusions

Co-Mn/CeO_2 was first prepared and used as a heterogeneous ozone catalyst. Co-Mn/CeO_2 had a disordered mesostructure and its performance was good in the catalytic ozonation for NOR removal, especially in mineralization. With the addition of Co-Mn/CeO_2, the removal efficiency of TOC significantly increased from 3.33% to 36.31%, compared to single ozonation. The dosage of ozone, the dosage of NOR, the dosage of the catalyst and the solution pH have different effects on the degradation of NOR. In catalytic ozonation, the degradation efficiency of NOR was higher at a basic pH than that at neutral or acid pH values. The removal of NOR was highest at a pH value of 9, Co-Mn/CeO_2 dosage of 0.8 g/L and O_3 concentration of 300 mL/min. Co-Mn/CeO_2 also showed good stability and can be reused five times without significant catalytic activity loss. This research shows an efficient way to modify CeO_2 to remove organic pollution from wastewater through a catalytic ozonation process.

Author Contributions: R.L.: Investigation, Methodology, Validation, Software, Formal analysis, Data curation, Writing—Original draft writing. J.X.: Supervision, Validation, Conceptualization Y.Z.: Conceptualization, Methodology, Writing—Review and editing, Supervision, Formal analysis, Validation, Project administration, Funding acquisition. S.W.: Resources, Supervision. H.Z.: Supervision, Software. L.L.: Supervision, Software. All authors have read and agreed to the published version of the manuscript.

Funding: This research was funded by the Natural Science Foundation of Guangxi Province (2020GXNSFAA159135), the Foundation (No.2021KF05) of Guangxi Key Laboratory of Clean Pulp & Papermaking and Pollution Control, National Natural Science Foundation of China (NSFC No: 21968005), Innovation Project of Guangxi Graduate Education (YCSW2022055), Guangxi Ba-Gui Scholars Program(2019A33), the foundation of Guangxi Key Laboratory of Clean Pulp & Papermaking and Pollution Control (ZR201702), 2019 Yongjiang Plan Project—Pulp and Paper Industry AOX Ultra-low Emission Technology Development and Application Demonstration (2019003), College of Light Industry and Food Engineering, Guangxi University.

Data Availability Statement: Not applicable.

Conflicts of Interest: The authors declare no conflict of interest.

References

1. Zhang, Y.; Xiao, R.; Wang, S.; Zhu, H.; Song, H.; Chen, G.; Lin, H.; Zhang, J.; Xiong, J. Oxygen vacancy enhancing Fenton-like catalytic oxidation of norfloxacin over prussian blue modified CeO_2: Performance and mechanism. *J. Hazard. Mater.* **2020**, *398*, 122863. [CrossRef]
2. Chen, H.; Wang, J. MOF-derived Co_3O_4-C@FeOOH as an efficient catalyst for catalytic ozonation of norfloxacin. *J. Hazard. Mater.* **2021**, *403*, 123697. [CrossRef]
3. Wang, G.; Zhao, D.; Kou, F.; Ouyang, Q.; Chen, J.; Fang, Z. Removal of norfloxacin by surface Fenton system ($MnFe_2O_4/H_2O_2$): Kinetics, mechanism and degradation pathway. *Chem. Eng. J.* **2018**, *351*, 747–755. [CrossRef]
4. Wang, Y.; Wang, R.; Lin, N.; Xu, J.; Liu, X.; Liu, N.; Zhang, X. Degradation of norfloxacin by MOF-derived lamellar carbon nanocomposites based on microwave-driven Fenton reaction: Improved Fe(III)/Fe(II) cycle. *Chemosphere* **2022**, *293*, 133614. [CrossRef]
5. Larsson, D.G.; de Pedro, C.; Paxeus, N. Effluent from drug manufactures contains extremely high levels of pharmaceuticals. *J. Hazard. Mater.* **2007**, *148*, 751–755. [CrossRef]
6. Li, H.; Chen, J.; Hou, H.; Pan, H.; Ma, X.; Yang, J.; Wang, L.; Crittenden, J.C. Sustained molecular oxygen activation by solid iron doped silicon carbide under microwave irradiation: Mechanism and application to norfloxacin degradation. *Water Res.* **2017**, *126*, 274–284. [CrossRef]
7. Zhang, X.-W.; Wang, F.; Wang, C.-C.; Wang, P.; Fu, H.; Zhao, C. Photocatalysis activation of peroxodisulfate over the supported Fe_3O_4 catalyst derived from MIL-88A(Fe) for efficient tetracycline hydrochloride degradation. *Chem. Eng. J.* **2021**, *426*, 131927. [CrossRef]
8. Yu, D.; Wu, M.; Hu, Q.; Wang, L.; Lv, C.; Zhang, L. Iron-based metal-organic frameworks as novel platforms for catalytic ozonation of organic pollutant: Efficiency and mechanism. *J. Hazard. Mater.* **2019**, *367*, 456–464. [CrossRef]
9. Miao, H.F.; Cao, M.; Xu, D.Y.; Ren, H.Y.; Zhao, M.X.; Huang, Z.X.; Ruan, W.Q. Degradation of phenazone in aqueous solution with ozone: Influencing factors and degradation pathways. *Chemosphere* **2015**, *119*, 326–333. [CrossRef]
10. Dantas, R.F.; Contreras, S.; Sans, C.; Esplugas, S. Sulfamethoxazole abatement by means of ozonation. *J. Hazard. Mater.* **2008**, *150*, 790–794. [CrossRef]
11. Li, P.; Zhan, S.; Yao, L.; Xiong, Y.; Tian, S. Highly porous alpha-MnO_2 nanorods with enhanced defect accessibility for efficient catalytic ozonation of refractory pollutants. *J. Hazard. Mater.* **2022**, *437*, 129235. [CrossRef] [PubMed]
12. Afzal, S.; Quan, X.; Lu, S. Catalytic performance and an insight into the mechanism of CeO_2 nanocrystals with different exposed facets in catalytic ozonation of p-nitrophenol. *Appl. Catal. B Environ.* **2019**, *248*, 526–537. [CrossRef]
13. Nawaz, F.; Cao, H.; Xie, Y.; Xiao, J.; Chen, Y.; Ghazi, Z.A. Selection of active phase of MnO_2 for catalytic ozonation of 4-nitrophenol. *Chemosphere* **2017**, *168*, 1457–1466. [CrossRef] [PubMed]
14. Heuer, J.; Ferguson, C.T.J. Photocatalytic polymer nanomaterials for the production of high value compounds. *Nanoscale* **2022**, *14*, 1646–1652. [CrossRef]
15. Hien, N.T.; Nguyen, L.H.; Van, H.T.; Nguyen, T.D.; Nguyen, T.H.V.; Chu, T.H.H.; Nguyen, T.V.; Trinh, V.T.; Vu, X.H.; Aziz, K.H.H. Heterogeneous catalyst ozonation of Direct Black 22 from aqueous solution in the presence of metal slags originating from industrial solid wastes. *Sep. Purif. Technol.* **2020**, *233*, 115961. [CrossRef]
16. Hama Aziz, K.H. Application of different advanced oxidation processes for the removal of chloroacetic acids using a planar falling film reactor. *Chemosphere* **2019**, *228*, 377–383. [CrossRef]
17. He, Y.; Wang, L.; Chen, Z.; Shen, B.; Wei, J.; Zeng, P.; Wen, X. Catalytic ozonation for metoprolol and ibuprofen removal over different MnO_2 nanocrystals: Efficiency, transformation and mechanism. *Sci. Total Environ.* **2021**, *785*, 147328. [CrossRef]
18. Álvarez, P.M.; Beltrán, F.J.; Pocostales, J.P.; Masa, F.J. Preparation and structural characterization of Co/Al2O3 catalysts for the ozonation of pyruvic acid. *Appl. Catal. B Environ.* **2007**, *72*, 322–330. [CrossRef]
19. Piumetti, M.; Bensaid, S.; Russo, N.; Fino, D. Nanostructured ceria-based catalysts for soot combustion: Investigations on the surface sensitivity. *Appl. Catal. B Environ.* **2015**, *165*, 742–751. [CrossRef]
20. Mann, A.K.P.; Wu, Z.; Calaza, F.C.; Overbury, S.H. Adsorption and Reaction of Acetaldehyde on Shape-Controlled CeO_2 Nanocrystals: Elucidation of Structure–Function Relationships. *ACS Catal.* **2014**, *4*, 2437–2448. [CrossRef]

21. Zheng, M.; Wang, S.; Li, M.; Xia, C. H_2 and CO oxidation process at the three-phase boundary of Cu-ceria cermet anode for solid oxide fuel cell. *J. Power Source* **2017**, *345*, 165–175. [CrossRef]
22. Izu, N.; Itoh, T.; Shin, W.; Matsubara, I.; Murayama, N. The effect of hafnia doping on the resistance of ceria for use in resistive oxygen sensors. *Sens. Actuators B Chem.* **2007**, *123*, 407–412. [CrossRef]
23. Govinda Rao, B.; Jampaiah, D.; Venkataswamy, P.; Reddy, B.M. Enhanced Catalytic Performance of Manganese and Cobalt Co-doped CeO2Catalysts for Diesel Soot Oxidation. *ChemistrySelect* **2016**, *1*, 6681–6691. [CrossRef]
24. Wang, J.; Quan, X.; Chen, S.; Yu, H.; Liu, G. Enhanced catalytic ozonation by highly dispersed CeO_2 on carbon nanotubes for mineralization of organic pollutants. *J. Hazard. Mater.* **2019**, *368*, 621–629. [CrossRef] [PubMed]
25. Chen, X.; Zhan, S.; Chen, D.; He, C.; Tian, S.; Xiong, Y. Grey Fe-CeO2-σ for boosting photocatalytic ozonation of refractory pollutants: Roles of surface and bulk oxygen vacancies. *Appl. Catal. B Environ.* **2021**, *286*, 119928. [CrossRef]
26. Akhtar, J.; Amin, N.S.; Aris, A. Combined adsorption and catalytic ozonation for removal of sulfamethoxazole using Fe_2O_3/CeO_2 loaded activated carbon. *Chem. Eng. J.* **2011**, *170*, 136–144. [CrossRef]
27. Li, S.; Tang, Y.; Chen, W.; Hu, Z.; Li, X.; Li, L. Heterogeneous catalytic ozonation of clofibric acid using Ce/MCM-48: Preparation, reaction mechanism, comparison with Ce/MCM-41. *J. Colloid Interface Sci.* **2017**, *504*, 238–246. [CrossRef]
28. Mo, S.; Li, J.; Liao, R.; Peng, P.; Li, J.; Wu, J.; Fu, M.; Liao, L.; Shen, T.; Xie, Q.; et al. Unraveling the decisive role of surface CeO_2 nanoparticles in the Pt-CeO_2/MnO_2 hetero-catalysts for boosting toluene oxidation: Synergistic effect of surface decorated and intrinsic O-vacancies. *Chem. Eng. J.* **2021**, *418*, 129399. [CrossRef]
29. Zhu, C.; Wei, X.; Li, W.; Pu, Y.; Sun, J.; Tang, K.; Wan, H.; Ge, C.; Zou, W.; Dong, L. Crystal-Plane Effects of CeO_2{110} and CeO2{100} on Photocatalytic CO2 Reduction: Synergistic Interactions of Oxygen Defects and Hydroxyl Groups. *ACS Sustain. Chem. Eng.* **2020**, *8*, 14397–14406. [CrossRef]
30. Du, X.; Dai, Q.; Wei, Q.; Huang, Y. Nanosheets-assembled Ni (Co) doped CeO_2 microspheres toward NO + CO reaction. *Appl. Catal. A Gen.* **2020**, *602*, 117728. [CrossRef]
31. Todorova, S.; Kolev, H.; Holgado, J.P.; Kadinov, G.; Bonev, C.; Pereñíguez, R.; Caballero, A. Complete n-hexane oxidation over supported Mn–Co catalysts. *Appl. Catal. B Environ.* **2010**, *94*, 46–54. [CrossRef]
32. Faria, P.C.; Monteiro, D.C.; Orfao, J.J.; Pereira, M.F. Cerium, manganese and cobalt oxides as catalysts for the ozonation of selected organic compounds. *Chemosphere* **2009**, *74*, 818–824. [CrossRef] [PubMed]
33. Song, H.; Hu, F.; Peng, Y.; Li, K.; Bai, S.; Li, J. Non-thermal plasma catalysis for chlorobenzene removal over $CoMn/TiO_2$ and CeMn/TiO2: Synergistic effect of chemical catalysis and dielectric constant. *Chem. Eng. J.* **2018**, *347*, 447–454. [CrossRef]
34. Zhou, G.; He, X.; Liu, S.; Xie, H.; Fu, M. Phenyl VOCs catalytic combustion on supported CoMn/AC oxide catalyst. *J. Ind. Eng. Chem.* **2015**, *21*, 932–941. [CrossRef]
35. Lu, J.; Sun, J.; Chen, X.; Tian, S.; Chen, D.; He, C.; Xiong, Y. Efficient mineralization of aqueous antibiotics by simultaneous catalytic ozonation and photocatalysis using $MgMnO_3$ as a bifunctional catalyst. *Chem. Eng. J.* **2019**, *358*, 48–57. [CrossRef]
36. Yu, D.; Wang, L.; Yang, T.; Yang, G.; Wang, D.; Ni, H.; Wu, M. Tuning Lewis acidity of iron-based metal-organic frameworks for enhanced catalytic ozonation. *Chem. Eng. J.* **2021**, *404*, 127075. [CrossRef]
37. Yu, H.; Ge, P.; Chen, J.; Xie, H.; Luo, Y. The degradation mechanism of sulfamethoxazole under ozonation: A DFT study. *Environ. Sci. Process Impacts* **2017**, *19*, 379–387. [CrossRef]
38. Zhang, C.; Wang, K.; Xie, K.; Han, X.; Ma, W.; Li, X.; Teng, G. Controllable preparation of hierarchical MnCo bimetallic photocatalyst and the effect of atomic ratio on its photocatalytic activity. *Chem. Eng. J.* **2022**, *446*, 136907. [CrossRef]
39. Rong, S.; Zhang, P.; Liu, F.; Yang, Y. Engineering Crystal Facet of α-MnO_2 Nanowire for Highly Efficient Catalytic Oxidation of Carcinogenic Airborne Formaldehyde. *ACS Catal.* **2018**, *8*, 3435–3446. [CrossRef]
40. Feng, N.; Zhu, Z.; Zhao, P.; Wang, L.; Wan, H.; Guan, G. Facile fabrication of trepang-like CeO_2@MnO_2 nanocomposite with high catalytic activity for soot removal. *Appl. Surf. Sci.* **2020**, *515*, 146013. [CrossRef]
41. Feng, Z.; Ren, Q.; Peng, R.; Mo, S.; Zhang, M.; Fu, M.; Chen, L.; Ye, D. Effect of CeO_2 morphologies on toluene catalytic combustion. *Catal. Today* **2019**, *332*, 177–182. [CrossRef]
42. Mohebali, H.; Moussavi, G.; Karimi, M.; Giannakis, S. Catalytic ozonation of Acetaminophen with a magnetic, Cerium-based Metal-Organic framework as a novel, easily-separable nanocomposite. *Chem. Eng. J.* **2022**, *434*, 134614. [CrossRef]
43. Li, S.; Huang, J.; Ye, Z.; Wang, Y.; Li, X.; Wang, J.; Li, L. The mechanism of Metal-H_2O_2 complex immobilized on MCM-48 and enhanced electron transfer for effective peroxone ozonation of sulfamethazine. *Appl. Catal. B Environ.* **2021**, *280*, 119453. [CrossRef]
44. Qi, F.; Chu, W.; Xu, B. Ozonation of phenacetin in associated with a magnetic catalyst $CuFe_2O_4$: The reaction and transformation. *Chem. Eng. J.* **2015**, *262*, 552–562. [CrossRef]
45. Wang, J.; Bai, Z. Fe-based catalysts for heterogeneous catalytic ozonation of emerging contaminants in water and wastewater. *Chem. Eng. J.* **2017**, *312*, 79–98. [CrossRef]
46. Chen, H.; Zhang, Z.; Hu, D.; Chen, C.; Zhang, Y.; He, S.; Wang, J. Catalytic ozonation of norfloxacin using Co_3O_4/C composite derived from ZIF-67 as catalyst. *Chemosphere* **2021**, *265*, 129047. [CrossRef]
47. Wang, X.; Sun, Y.; Yang, L.; Shang, Q.; Wang, D.; Guo, T.; Guo, Y. Novel photocatalytic system Fe-complex/TiO_2 for efficient degradation of phenol and norfloxacin in water. *Sci. Total Environ.* **2019**, *656*, 1010–1020. [CrossRef]